DOI 10.5012/bkcs.2011.32.6.2027

Molecular Dynamics Study on the Binary Collision of Nanometer-Sized Droplets of Liquid Argon

Inbeom Chun, Man Yeong Ha, Joonkyung Jang,†,* and Hyun Sik Yoon‡

*School of Mechanical Engineering, †Department of Nanomaterials Engineering, and ‡Advanced Ship Engineering Research center, Pusan National University, Busan 609-735, Korea. *E-mail: jkjang@pusan.ac.kr*
Received February 28, 2011, Accepted April 26, 2011

Molecular dynamics simulation is used to study the binary collisions of nanometer-sized droplets of argon in the presence of a surrounding gas. By systematically varying the droplet size, the impact parameter and the velocity of collision, the outcome of such collisions were examined and they can be classified into coalescence, separation and shattering. If one of the colliding droplets is half or less than the other in diameter, a shattering is not possible to occur. The threshold of impact parameter for a given separation was studied by adjusting the Weber number. Overall nanoscale droplets were more likely to coalesce than the macroscopic sized ones due to their high surface-to-volume ratio.

Key Words : Nanometer droplet collision, Molecular dynamics, Coalescence, Shattering

Introduction

Droplets collisions are commonly occurred in the growth of rain drops and spray combustions such as direct gasoline injection.[1,2] Efforts have been made to understand these collisions in terms of various physicochemical properties and geometrical shapes. Brazier-Smith *et al*.[3] experimentally studied collisions between macroscopic sized water droplets (the drop radius ranging from 0.15 to 0.75 mm), and the results could be categorized into 3 different mechanisms: coalescence, bouncing, and separation.[3] The occurrence of each mechanism largely depended on factors such as the ratio of droplet radii, the impact parameter, the relative velocity of collision, the surface tension and the density of the droplet. In this case theoretical calculations can be used to provide useful predictions for the droplet motion, and therefore the collision of the liquid droplets was studied by the smoothed particle hydrodynamics[4] and lattice Boltzmann method.[5]

The collisions between nanometer-sized droplets are of key importance since they are the prerequisite of a macroscopic drop formation. Due to the high surface-to-volume ratio of these nanodroplets, their collisions can be different from those of the macroscopic ones. As this problem could not be solved by experimental investigations, a molecular dynamics (MD) simulation was merged into this study as a viable option. MD simulations have been conducted for various droplets including argon,[6,7] water,[8,9] and other generic non-polar atoms or molecules.[10] Varying the velocity and the impact parameter of the collision[6] could result to droplet coalescence, stretched separation, or shattering. In the presence of an ambient gas, a bouncing mechanism of the droplets was also found.[7] These possible outcomes are similar to those from macroscopic droplet collisions, except differing in size as shown in the MD simulation below. It is obvious that a droplet is a collection of molecules but not a continuum body as assumed in the hydrodynamics and lattice Boltzmann methods. These continuum pictures of droplet are valid for macroscopic droplets only. Therefore, a molecular dynamics simulation seems appropriate for the present nanodroplets.

In general, the colliding droplets differ in size, despite MD simulations published in many literature only focused on droplets of equal size.[6,8] In addition it was reported that an ambient gas plays a significant role in the collision.[7] In light of this, the collision of argon droplets differing in size are studied by explicitly considering the presence of an ambient gas. By systematically varying the size of droplet as well as the velocity and impact parameter of collision, the resulting collision can be classified into different scattering channels. Furthermore the impact parameter threshold for the transition from coalescence to separation was expressed as a function of Weber number (WN). Consequently these threshold values are compared with those of the macroscopic drops.

Simulation Methods

The interatomic interaction was modeled by the pairwise Lennard-Jones (LJ) potential,[11]

$$U_{LJ} = 4\varepsilon\left[\left(\frac{\sigma}{r}\right)^{12} - \left(\frac{\sigma}{r}\right)^{6}\right] \quad (1)$$

where ε and σ are the well depth and the equilibrium distance of the potential, respectively, and r is the interatomic distance. The cutoff distance of the LJ potential was 2.5σ, and the long-range correction was achieved by shifting the LJ potential.[11] The velocity Verlet algorithm was applied for propagation of MD trajectories.[12]

Droplets of Ar consisting of 144 to 1,772 atoms were generated as follows. First starting from the face centered cubic lattice of Ar, a constant temperature (NVT) MD

simulation was run at 84 K for 100-600 ps. The initially solid-like argon melted and became a spherical liquid droplet. From which the density profile of the droplet was plotted in Figure 1(a). The radius of the droplet r_e is determined by fitting the density profile along the radial direction $\rho(r)$ to the hyperbolic tangent function,

$$\rho(r) = \frac{1}{2}(\rho^l + \rho^v) - \frac{1}{2}(\rho^l - \rho^v)\tanh\left(\frac{2(r - r_e)}{d}\right), \quad (2)$$

where ρ^l and ρ^v are the liquid and vapor densities of Ar, and d is the width of droplet boundary. The density profile obtained from MD simulation was fitted by varying the ρ^l and ρ^v, r_e, and the d. A nonlinear fitting to obtain these four variables was performed. Figure 1(b) shows $\rho(r)$ (in circles) and its best fit (solid line) where the droplet radius in this case was r_e = 18.75 Å.

The binary collision of droplets (Figure 1(c)) was simulated by a constant energy (NVE) MD method.[11] The first step was to set up a rectangular simulation box with a volume of 400 × 200 × 200 Å^3 (the length of the box was the direction of collision, Figure 1(c)) by applying the periodic boundary conditions. After that, the collision velocity V_{rel} was imposed by adding $V_{rel}/2$ to the center of mass (CM) velocity of each droplet in its moving direction (Figure 1(c)). The impact parameter X was defined as

$$X = \frac{B}{R_1 + R_2}, \quad (3)$$

where R_1 and R_2 are the radii of the larger and smaller droplets in collision, respectively. B is defined as the distance between the two lines along which the CMs of colliding droplets are moving. X = 0 corresponds to a head-on collision, and X = 1 to the case where two droplets graze each other. X was varied from 0 to 1 in the simulation. In addition the ratio of droplet radii R_r (= R_2/R_1) varied as 0.5, 0.75, and 1.0. WN is defined as

$$WN = \frac{\rho V_{rel}^2 D_z}{\gamma_z} \quad (4)$$

where ρ is the mass density of the droplet, and D_z and γ_z are the diameter and surface tension of the smaller droplet, respectively (we used the experimental value of the surface tension). WN ranged from 20 to 450. For a given WN, the binary collision of equal-sized droplets results in coalescence or separation depending on X values (high X s give separation). Brazier-Smith *et al.*[3] derived an equation of the threshold X value for separation X_c as

$$X_c = \frac{c}{\sqrt{WN}}\sqrt{\frac{1.25}{R_r} + 0.05}, \quad (5)$$

where c is empirically determined to be 2.191.

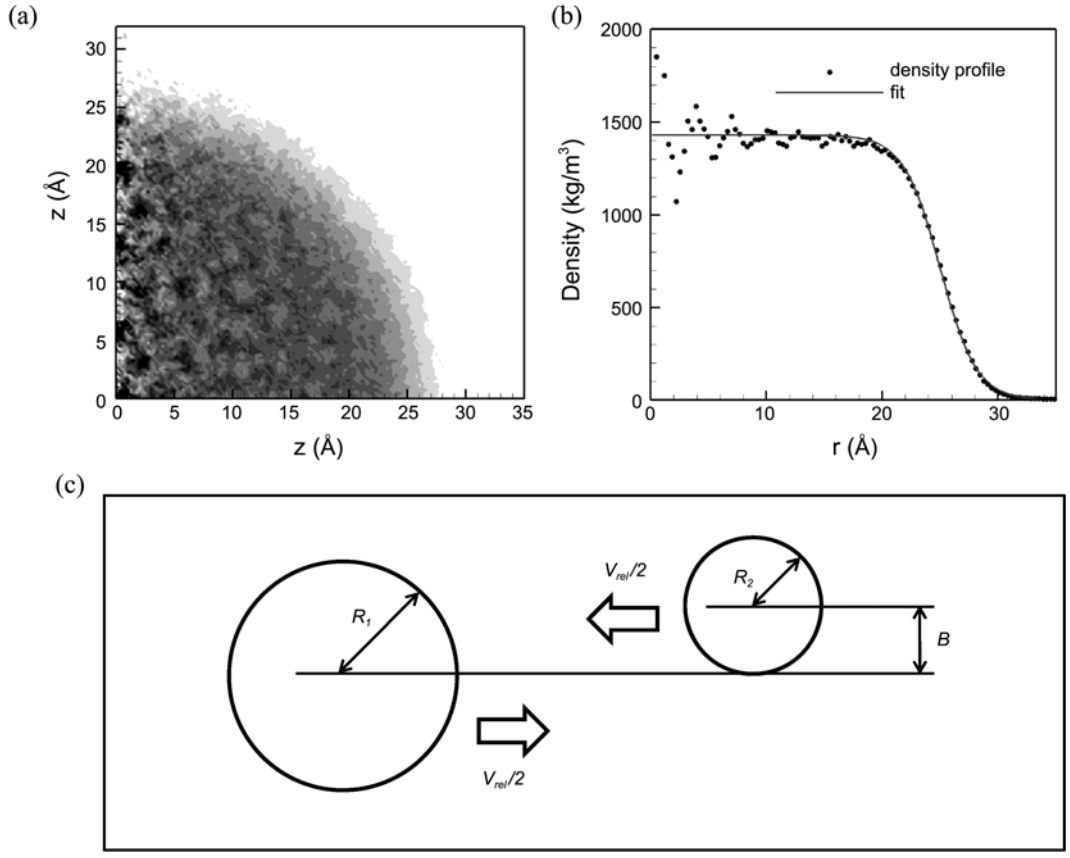

Figure 1. (a) Density profile of an argon droplet with a radius of 25 Å. The density profile was obtained by averaging snapshots over 400 ps. Only the first quadrant of the density profile is shown. (b) The density profile along the radial direction with its best fit by equation (2). (c) Schematics for the binary collision of droplets. Each line passes through the center of mass of the droplet and represents its moving direction. B is the distance between the two parallel lines. The half of the velocity $V_{rel}/2$ is added to each droplet along its moving direction.

Results and Discussions

Figure 2 illustrates various outcomes of the binary collision between equal-sized droplets (R_r = 1.0) for different X s and WNs, and the two droplets are colored differently for better distinguishability. After the head-on collision shown in Figure 2(a) (X = 0), the two spherical droplets merge into an ellipsoid as plotted in Figure 2(b). Depending on the WN, the merged droplet can branch into two different paths. If the WN is large (=420), the merged droplet is flattened out as in Figure 2(c), and finally it decomposes into both small and medium-sized fragments as illustrated in Figure 2(d). This process (Figure 2(a)→(b)→(c)→(d)) is classified as shattering. In contrast, if the WN is relatively small (=190), the merged droplet in Figure 2(b) remains as aggregates due to the domination of intermolecular cohesion over the inertial force of collision appeared in Figure 2(e). Therefore the merged droplet eventually becomes nearly spherical as shown in Figure 2(f). This process (Figure 2(a)→(b)→(e)→(f)) is defined as coalescence.

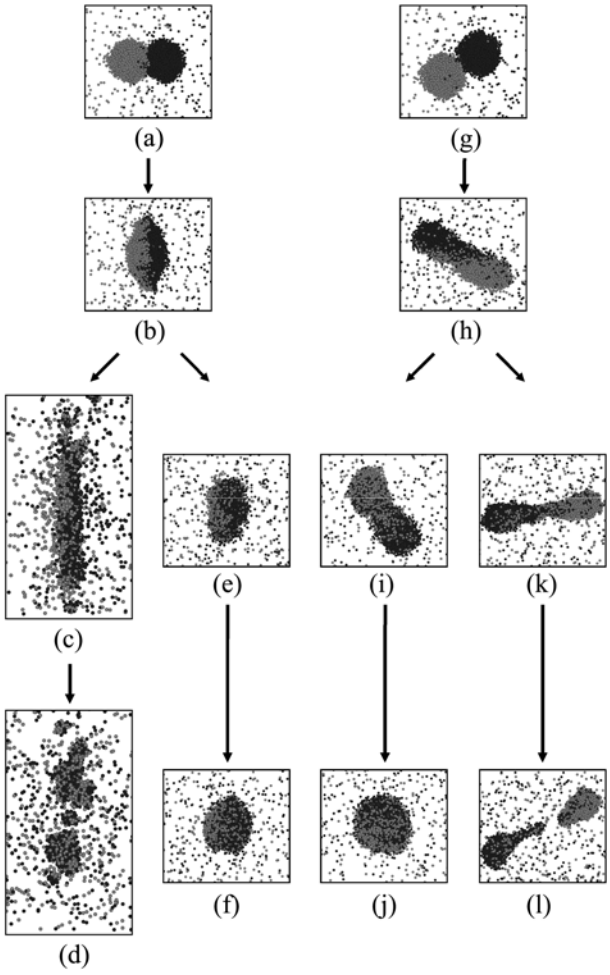

Figure 2. Diverse outcomes from the binary collisions of equal-sized droplets, R_r=1. Snapshots are shown for different X s and WNs. Two droplets are drawn in different colors. Shown in (d), (f), (j), and (l) are the results of collisions with WN=420 and X=0, WN=190 and X=0, WN=170 and X=0.4, and, WN=170 and X=0.5, respectively.

Figure 2(g) presents an off-centered (X = 0.4) collision of equal-sized droplets. The droplets fuse into a dumbbell and rotate counterclockwise with respect to their CM as shown in Figure 2(h). If WN=170 and X = 0.4, the merged droplet gradually contracts while rotating as shown in Figure 2(i). It finally becomes spherical in shape as plotted in Figure 2(j), giving rise to the coalescence of the droplets (Figure 2(g)→(h)→(i)→(j)). However if the impact parameter X increases to 0.5 by fixing WN, the inertial force of collision dominates, and hence the merged droplets stretch out as in Figure 2(k), which eventually break down into two separate droplets (Figure 2(l)). This process (Figure 2(g)→(h)→(k)→(l)) is named as stretched separation.

To investigate the effect of R_r values, the binary collision for R_r=0.75 was studied, and the outcomes were similar to those for R_r=1.0 (shattering, coalescene, or separation). However, when R_r was further reduced to 0.5, only coalescence and separation were observed (Figure 3). A head-on collision gave rise to a merged droplet nearly hemispherical in shape (Figure 3(b)). With time, the hemispherical droplet progressively transformed into an ellipsoid (Figure 3(c)) and

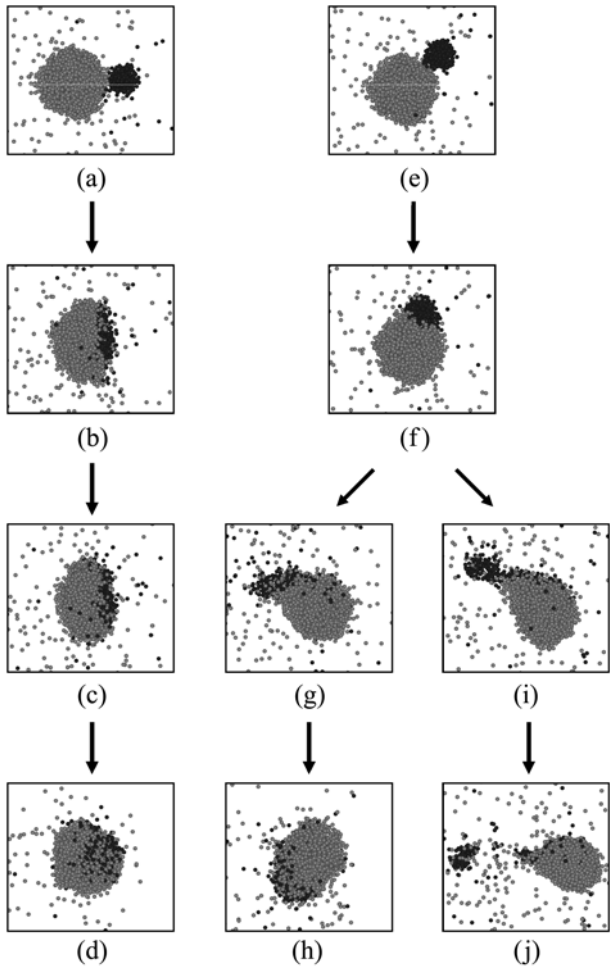

Figure 3. Diverse outcomes from the binary collisions of unequal droplets, R_r=0.5. Snapshots are shown for different X s and WNs. Two droplets are drawn in different colors. Shown in (d), (h), and (j) are the results of collisions with WN=190 and X=0, WN=190 and X=0.4, and WN=420 and X=0.5, respectively.

then into a sphere (Figure 3(d)). Unlike for R_r=0.75 and 1, coalescence is occurred in this case (Figure 3(a)→(b)→(c)→(d)).

Figure 3(e) illustrates an off-centered collision with X=0.4. The smaller droplet fuses into a larger one followed by counterclockwise rotation as in Figure 3(f). For a WN of 190, the rotating droplet shrinks as shown in Figure 3(g) and finally reached a near spherical shape (Figure 3(h)). This process (Figure 3(e)→(f)→(g)→(h)) is coalescence as found for R_r=0.75 and 1. If X is increased to 0.5 (Figure 3(i)), the merged droplet are stretched and it eventually break into two separate droplets as shown in Figure 3(j), leading to a separation.

By systematically varying X and WN, the resulting collisions were classified into 3 scattering channels: coalescence, separation, and shattering. Such a classification for R_r=0.75 is shown in Figure 4(a). For WN < 320, coalescence or stretched separation occurs depending on X. One can clearly see the boundary between coalescence and separation regions. The threshold X for the transition from coalescence to separation decreases with increasing WN. If WN > 320, the coalescence vanishes, and shattering occurs instead. On comparison the threshold X for the shattering increases with increasing WN (not drawn here). The same qualitative behavior is found for R_r=1.0 and 0.5, except that shattering is not observed for R_r=0.5. Figure 4(b) shows the threshold X for the stretched separation as a function of WN in the case of R_r=1.0. Our results (filled circles) agree with the previous reported results by Ming *et al.*[6] (open circles). Additionally the best fit to our results was also plotted in the same figure using equation (5).

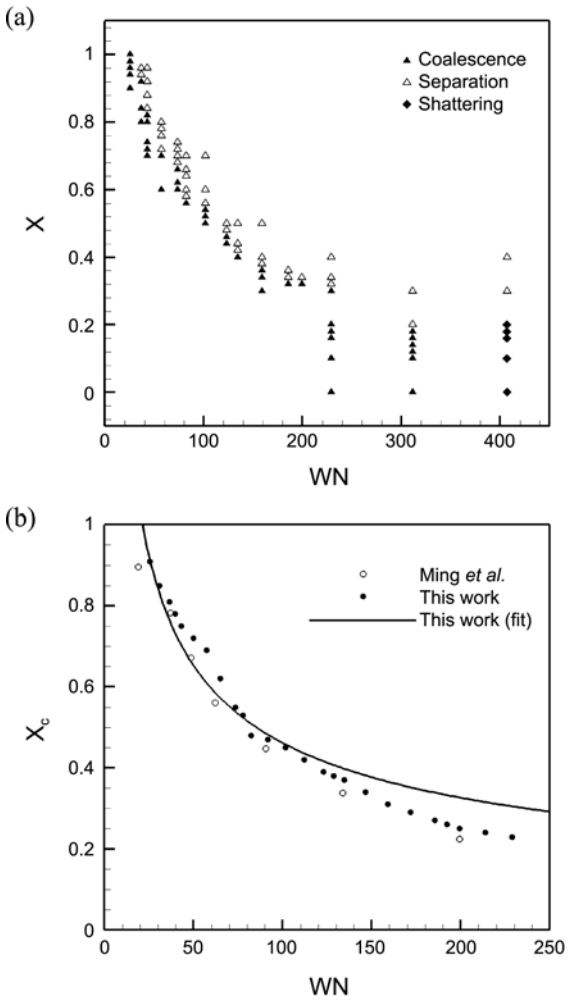

Figure 4. Classification of collision into three different scattering channels for R_r=0.75 (a). The threshold of impact parameter for separation X_c *vs*. WN and its fit using equation (5) for R_r=1.0 (b). The previous result reported by Ming *et al.* is shown for comparison.

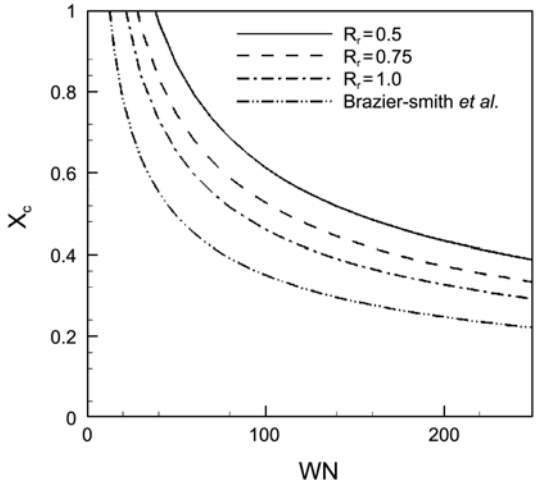

Figure 5. The threshold impact parameter X_c *vs*. WN for R_r s of 1.0, 0.75, and 0.5. The curve obtained for the macroscopic limit by Brazier-Smith *et al.* is shown for comparison.

In general X_c vs. WN and its fit (as shown in Figure 4(b)) for the collisions of droplets with different sizes (R_r=0.75, 0.5) were obtained. Figure 5 plots such fits for R_r=0.5, 0.75 and 1.0. Also drawn in the figure is equation (5) derived by Brazier-Smith *et. al* for the collision of macroscopic drops. The X_c curves for the present nanodroplets are shifted upward compared to that for macroscopic drops. The values of *c* in equation (5) are 3.842, 4.017 and 4.048 for R_r=0.5, 0.75 and 1.0, respectively (*c*=2.191 for the macroscopic limit). Therefore, with the reduction of the droplet size, the merged droplet under impact tends to separate at a larger value of X or WN. This implies that nanodroplets coalesce more easily than the macroscopic drops. This is due to the increased cohesion of the smaller droplets which in turn arises from the increased surface tension as the result of their sizes. The collision with R_r=0.5 involves the smallest droplet, and consequently has the highest surface tension leading to the highest tendency of coalescence. The corresponding X_c is subsequently shifted up most.

We have not observed a bouncing of two droplets as observed in the previous simulation taking into account the presence of an ambient gas in the droplet collision. Therefore, the role of an ambient gas is minor in the present case. However, we need to run a simulation without the presence of an ambient gas and compare the results with the present simulation.

Conclusions

By using MD simulations, we studied the colliding droplets of liquid argon in the presence of a surrounding gas, and investigated the effect of WNs (20-450), impact parameters ($0 \le X \le 1$), droplet sizes. The collision behavior was defined into coalescence, separation, and shattering. Of which shattering is not observed if the ratio of droplet radii is 0.5 or smaller, regardless of the collision velocity. In addition the threshold impact parameter for the transition from coalescence to separation was also studied. As the size of droplet decreases, this threshold for a given WN increases. Therefore, nm-sized droplets coalesce more easily than macroscopic drops, and this is due to the increased surface tension (or surface to volume ratio) of nanoscaled droplets.

Acknowledgments. This work was supported by the National Research Foundation of Korea (NRF) grant funded by the Korea Government (No. 2010-0028251) and Leading Foreign Research Institute Recruitment Program through the NRF funded by the Ministry of Education, Science, and Technology (MEST) (No. K20702001648-10E0100-07010).

References

1. Adam, J. R.; Lindblad, N. R.; Hendricks, C. D. *J. Appl. Phys.* **1968**, *39*, 11.
2. Aneja, R.; Abraham, J. *Combustion Sci. Tech.* **1998**, *138*, 233.
3. Brazier-Smith, P. R.; Jennings, S. G.; Latham, J. *Proc. R. Soc. of London. Ser. A, Math. Phys. Sci.* **1972**, *326*, 393.
4. Meleán, Y.; Sigalotii, L.; Di G. *Int. J. Heat Mass Trans.* **2005**, *48*, 4041.
5. (a) Inamuro, T.; Ogata, T.; Tajima, S.; Konishi, N. *J. Comp. Phys.* **2004**, *198*, 628. (b) Sakakibara, B.; Inamuro, T. *Int. J. Heat Mass Trans.* **2008**, *51*, 3207.
6. Ming, L.; Markoviæ, N.; Svanberg, M.; Pettersson, J. B. C. *J. Phys. Chem. A* **1997**, *101*, 4011.
7. Murad, S.; Law, C. K. *Mol. Phys.* **1999**, *96*, 81.
8. Svanberg, M.; Ming, L.; Markoviæ, N.; Pettersson, J. B. C. *J. Chem. Phys.* **1998**, *108*, 5888.
9. Greenspan, D.; Heath, L. F. *J. Phys. D* **1991**, *24*, 91.
10. Yan, Y. Y.; Ji, C. Y. *J. Bionic Eng.* **2008**, *5*, 271.
11. Allen, M. P.; Tildesley, D. J. *Computer Simulation of Liquids*; Clarendon Press: Oxford, U.K., 1987.
12. Swope, W. C.; Andersen, H. C.; Berens, P. H.; Wilson, K. R. *J. Chem. Phys.* **1982**, *76*, 637.